Reversible Capture and Release of Cl2and Br2with a Redox-Active Metal-Organic Framework

UNIVERSITÀ DEGLI STUDI DI TORINO

Reversible Capture and Release of Elemental Halogens with a Redox-Active Metal-Organic Framework

Yuri Tulchinsky,[†] Christopher H. Hendon,[†] Kirill A. Lomachenko,[◊,ᵛ] Elisa Borfecchia,[§] Brent C. Melot,[♯] Matthew R. Hudson,[□] Jacob D. Tarver,[□,◦] Maciej D. Korzyński,[†] Amanda W. Stubbs,[†] Jacob J. Kagan, [‡] Carlo Lamberti,[§,ᵛ] Craig M. Brown,[□] and Mircea Dincă[†*]

[†] Department of Chemistry, Massachusetts Institute of Technology, 77 Massachusetts Avenue, Cambridge, Massachusetts, 02139, United States

[♯] Department of Chemistry, University of Southern California, 3620 McClintock Avenue, Los Angeles, California, 90089-1062, United States

[◊] European Synchrotron Radiation Facility, 71 Avenue des Martyrs, CS 40220, 38043 Grenoble Cedex 9, France

[ᵛ] IRC "Smart Materials", Southern Federal University, Zorge Street 5, 344090 Rostov-on-Don, Russia

[§] Department of Chemistry, NIS, CrisDi, and INSTM Centre of Reference, University of Turin, Via Quarello 15, I- 10135 Torino, Italy

[□] Center for Neutron Research, National Institute of Standards and Technology, Gaithersburg, USA

[◦] National Renewable Energy Laboratory, 15013 Denver West Parkway, Golden, USA

[‡] Department of Mathematics, Weizmann Institute of Science, 234 Herzl St., Rehovot, Israel

Abstract

Extreme toxicity, corrosiveness, and volatility pose serious challenges for the safe storage and transportation of elemental chlorine and bromine, which play critical roles in the chemical industry. Solid materials capable of forming stable non-volatile compounds upon reaction with elemental halogens may partially mitigate these challenges by allowing safe halogen release on demand. Here, we demonstrate that elemental halogens quantitatively oxidize coordinatively unsaturated Co(II) ions in a robust azolate metal-organic framework (MOF) to produce an air-stable and safe-to-handle Co(III) material featuring terminal Co(III)-halogen bonds. Thermal treatment of the oxidized MOF causes homolytic cleavage of the Co(III)-halogen bonds, reduction to Co(II), and concomitant release of elemental halogens. Remarkably, the reversible chemical storage and thermal release of elemental halogens occur with no significant losses of structural integrity, the parent cobaltous MOF retaining crystallinity and porosity even after three oxidation/reduction cycles. These results highlight a redox mechanism that may find utility in the storage and capture of other noxious and corrosive gases.

INTRODUCTION

Elemental halogens play key roles in a range of industrial processes. With an estimated annual production of 56 million tonnes, Cl_2 is widely used in water sanitation and is an essential ingredient in the production of plastics, such as polyvinylchloride and polyurethanes, as well as solvents and pesticides.[1] Albeit used on a comparatively smaller scale, Br_2 is a key element in flame retardants, agricultural products, and pharmaceuticals.[2] The irreplaceable role of the elemental halogens in industry is contrasted with their extreme toxicity, corrosiveness, and volatility, which pose serious challenges for their safe handling, storage, and transportation. Despite decades of experience in mitigating these challenges, tragic accidents still occur worldwide due to leaks or explosions, making the development of new materials that can enable the open-air, safe handling, and on-demand delivery of halogens highly desirable. Metal organic frameworks (MOFs), with their demonstrated utility in storing both inert and reactive gases, seem like logical choices for this challenge. However, despite of thousands of reports of gas sorption and storage in MOFs, many including oxidizing or corrosive gases such as O_2,[3,4] NO,[5] SO_2,[6,7] and NH_3,[7-10] none address the *reversible* storage of

Br_2 or Cl_2, to our knowledge. The closest example is the irreversible bromination of unsaturated organic ligand within a MOF, and subsequent release of HBr upon treatment with base.[11] The lack of reports on reversible storage of the gaseous halogens (i.e. excluding I_2) in MOFs is staggering given the interest in the field, but highlights the difficulty in isolating materials that can reversibly bind halogens and release them over at least several cycles.

Although physisorption is the most widely employed mechanism for gas storage in porous materials, it is less effective with the lighter halogens because gas retention under ambient conditions is relatively poor and thus still requires the use of specialized storage and handling equipment. One historical shortcoming of MOFs for this application is their chemical instability towards Cl_2 and Br_2. With reports of reversible redox cycling of MOFs,[12,13] we became intrigued by a chemical storage mechanism whereby Cl_2 and Br_2 could be stored by reduction to Cl^- and Br^-, and subsequently released by oxidation back to their elemental X_2 form. Here, we report such a mechanism, where elemental Br_2 and Cl_2 reversibly oxidize Co(II) centers in Co_2Cl_2BTDD (**1**, BTDD = bis(1H-1,2,3-triazolo[4,5-b],[4,5- i])dibenzo[1,4]dioxin) to form terminal Co(III)-halides in $Co_2Cl_2X_2$BTDD (X = Cl (**2**), Br (**3**)). Notably, these are the first examples of all-Co(III) MOFs. We show that the Co(III) materials can be reduced back to Co(II) thermally, with concomitant liberation of X_2. These results represent the first example of reversible halogen uptake and release with a MOF and portend applications for halogen capture in the context of toxic gas removal, and storage in the context of safe handling of halogens.

RESULTS AND DISCUSSION

Robust reactivity with elemental halogens and formation of all-Co(III) MOFs

Reaction of H_2BTDD with $CoCl_2 \cdot 6H_2O$ results in the formation of solvated Co_2Cl_2BTDD (**1**), as previously described.[10] Rietveld analysis of powder neutron diffraction data obtained from a sample of activated **1** at 10 K revealed a three-dimensional structure exhibiting one-dimensional channels arranged in a honeycomb fashion, similar to that reported for the Mn analog Mn_2Cl_2BTDD.[10] The secondary building units of **1** consist of infinite $–(Co–Cl)_n–$ chains coiled into threefold spirals and interconnected by the bis-triazolate linkers (Figure 1A). Reaction of olive-green rod-like microcrystals of **1** with gaseous Cl_2 or $PhICl_2$ in dichloromethane results in rapid oxidation and quantitative formation of dark brown microcrystals of Co_2Cl_4BTDD (**2**) (Figure 1B). A powder X-ray diffraction (PXRD) pattern of **2** revealed small but noticeable shifts of all the reflection peaks towards higher scattering angles, 2θ, most evident in the peaks corresponding to the (210) and (300) reflections (Figures 1C and S1), which shift from 4.5° and 7.8° in **1** to 4.6° and 8.0° in **2**, respectively. Neutron powder diffraction (NPD) analysis of **2** revealed decreases of 0.13 Å and 0.14 Å in the average Co–N and Co–Cl bond lengths, respectively, relative to **1**, as expected upon oxidation of Co(II) sites in **1** to Co(III) in **2**.

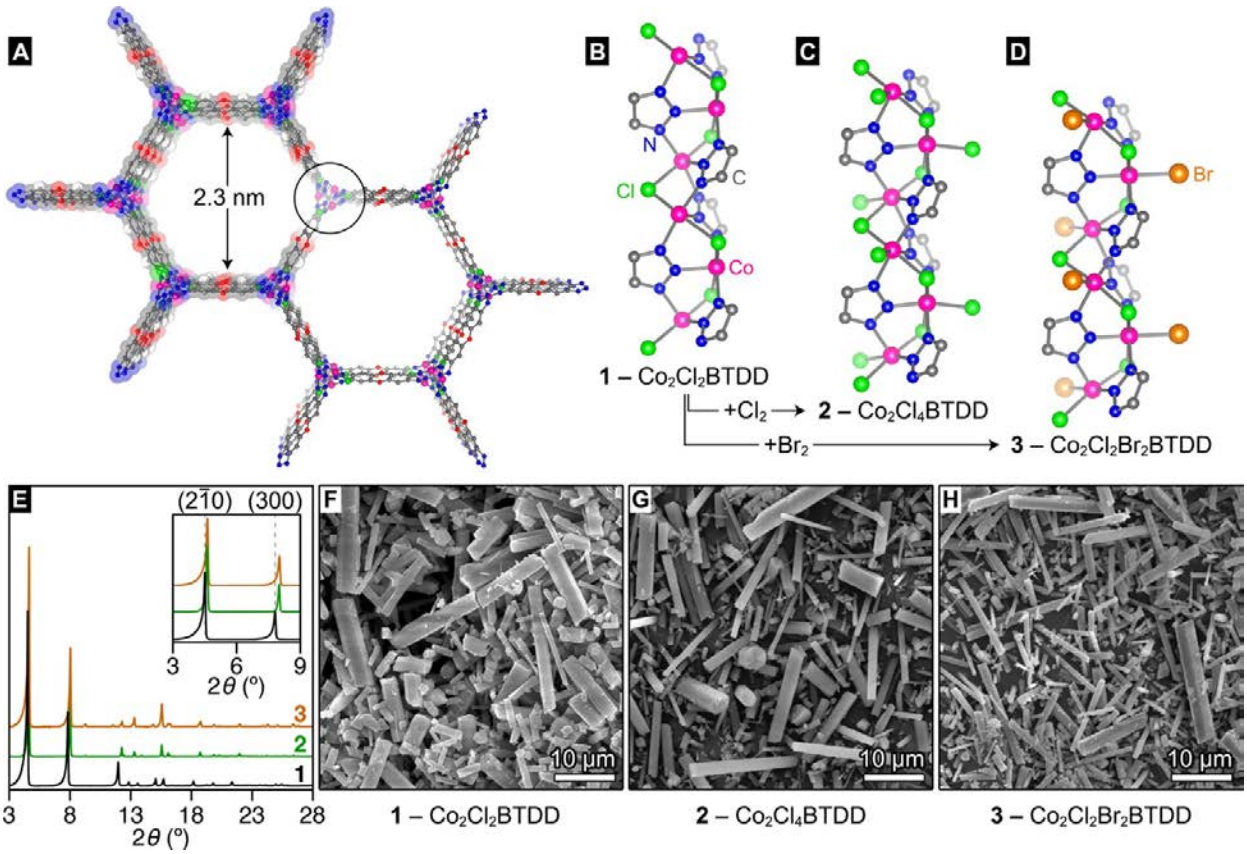

Figure 1. Structural and microscopy data. (A) A portion of the structure of the parent Co(II) MOF Co_2Cl_2BTDD (**1**) projected along the *c* axis. (B – D) SBU structures and local coordination environments of the Co centers in **1**, **2**, and **3**, respectively, as determined by NPD. (E) PXRD data for 1, 2, and 3 showing retention of crystallinity and the lattice contraction in moving from **1** to **2** and **3** as evidenced by the upshift in the 2θ values for the (100) and (001) reflections. (F – H) scanning electron micrographs of microcrystalline samples of **1**, **2**, and **3**, respectively.

The stoichiometry of the oxidation of **1** to **2** in the presence of Cl_2 or $PhICl_2$ was ascertained by microelemental analysis (see Supporting Information), X-ray absorption spectroscopy (XAS), and magnetometry. X-ray absorption near-edge spectra (XANES) at the Co K-edge of **1** and **2** at room temperature revealed that the absorption edge of **2** is shifted by approximately 2 eV to higher energy relative to **1** (Figure 2A).[14,15] Although this shift cannot be used to quantify the degree of oxidation in **1**, it does indicate a higher average effective nuclear charge on the metal. This confirms that oxidation indeed takes place at the Co centers and not at the ligand, as had been previously observed, for instance, with the topologically related Mn_2(2,5-dihydroxyterephthalate) (Mn-MOF-74) under similar oxidation conditions.[16] Magnetic measurements were particularly useful in determining whether oxidation of Co(II) centers in **1** to Co(III) is quantitative because the latter are expected to exhibit low spin (S = 0), whereas the former are paramagnetic. Temperature-dependent dc susceptibility measurements of **1** between 2 K and 300 K revealed typical Curie-Weiss behavior at 0.1 T. The susceptibility value at 300 K corresponds

to a total effective magnetic moment of μ_{eff} = 4.95 μ_B per Co, inferring high spin (S = 3/2) Co(II) centers (Figure S8). The magnetic behavior and effective moment of **1** are in line with those of the isostructural Co(II) system Co_2(2,5-dihydroxyterephthalate)$(H_2O)_2$ (Co-MOF-74, μ_{eff} = 4.67 μ_B).[17] The oxidized compound **2** showed a diamagnetic response at all but the lowest temperatures, as expected for a low spin d^6

complex in an octahedral crystal field. At 5 K, a small paramagnetic contribution is observed in the field-dependent low temperature magnetization plots (Figure S9). We attribute this paramagnetic signal to magnetically dilute residual Co(II) centers. Assuming that these exhibit an $S = 3/2$ ground state, the saturation magnetization value of 0.15 μ_B at 5 K and 13 T corresponds to a Co(II) content of approximately 2.5% in **2**. Repeated experiments revealed that the residual Co(II) content in **2** is consistently low, varying between 1% and 6%, depending on the batch and the number of consecutive treatments with oxidant. Thus, oxidation of **1** to **2** in the presence of Cl_2 or $PhICl_2$ is essentially quantitative, with isolated yields as high as 99%.

Elemental Br_2 is equally effective in oxidizing **1**. Prolonged exposure of **1** to Br_2 vapors results in quantitative conversion to $Co_2Cl_2Br_2$BTDD (**3**), whose composition and bromine content were confirmed by microelemental analysis and inductively-coupled plasma mass spectrometry (ICP-MS) after extensive vacuum treatment to remove unreacted, physisorbed Br_2 (Table S1). PXRD analysis of **3** revealed similar shifts of diffraction peaks as observed for **2**, with the most intense (210) and (300) reflections peaks shifting to 2□ values indistinguishable from those seen for **2** (Figures 1C, S1). Oxidation of **1** and formation of Co(III)-Br was further confirmed by NPD analysis of **3**, which revealed only scattering for the framework skeleton and the terminal Co(III)-bound bromide atoms and no significant scattering from inside the pores. Similarly to **2**, **3** exhibits noticeably shorter average Co–N and Co–Cl bonds relative to **1**:
1.92 Å vs. 2.12 Å and 2.34 Å vs. 2.40 Å, respectively, as expected for moving from Co(II) to Co(III). Quantitative oxidation of **1** was confirmed by allowing free occupancy of the terminal bromide site in the Rietveld refinement process, which gave best fits when the occupancy was 100%. Importantly, the neutron diffraction experiments revealed no structural disorder between the terminal bromides and the bridging chlorides originating from **1**. Indeed, allowing the possibility of full or partial interchange of the bridging and terminal halide positions did not improve the fit parameters, and in fact made them worse.

Oxidation of **1** by elemental halogens without bulk decomposition or microscopic framework collapse was also evidenced by scanning electron microscopy (SEM) and porosity measurements. Figures 1F-H show that microcrystals of **1** maintain their hexagonal rod-like shape upon oxidation. N_2 adsorption isotherms on **2** and **3** revealed saturation uptakes of 585 cm^3/g (306463 cm^3/mol) and 429 cm^3/g (262874 cm^3/mol), respectively, at 77 K (Figure S4). Fitting this data to the Barrett−Joyner−Halenda (BJH) pore size distribution model[18] with the Kruk-Jaroniec-Sayari correction for hexagonal pores[19] provides pore sizes of 20.5 Å and 20.3 Å for **2** and **3**, respectively (Figure S7). These are smaller than the pore size of **1**, 22.9 Å, and are in agreement with a pore narrowing due to the terminal halides protruding into the pores of the oxidized MOFs and the decreased unit cell parameters stemming from the smaller ionic radius of Co(III).

The robustness demonstrated by **1** in the presence of elemental Cl_2 and Br_2 is remarkable. Previous attempts to capture elemental Cl_2 in a MOF led to nearly complete loss of crystallinity of the parent materials.[20] We attribute the stability of **2** and **3** in part to the quantitative formation of kinetically inert low-spin Co(III) centers. Notably, MOFs made exclusively from Co(III) secondary building units (SBUs) are themselves unprecedented. Indeed, the only previous examples of MOFs containing Co(III) in the nodes are cases of mixed-valent Co(II)/Co(III) materials,[21-23] or examples where the presence of dilute Co(III) within a native Co(II) MOF has been inferred from its catalytic activity.[24-25]

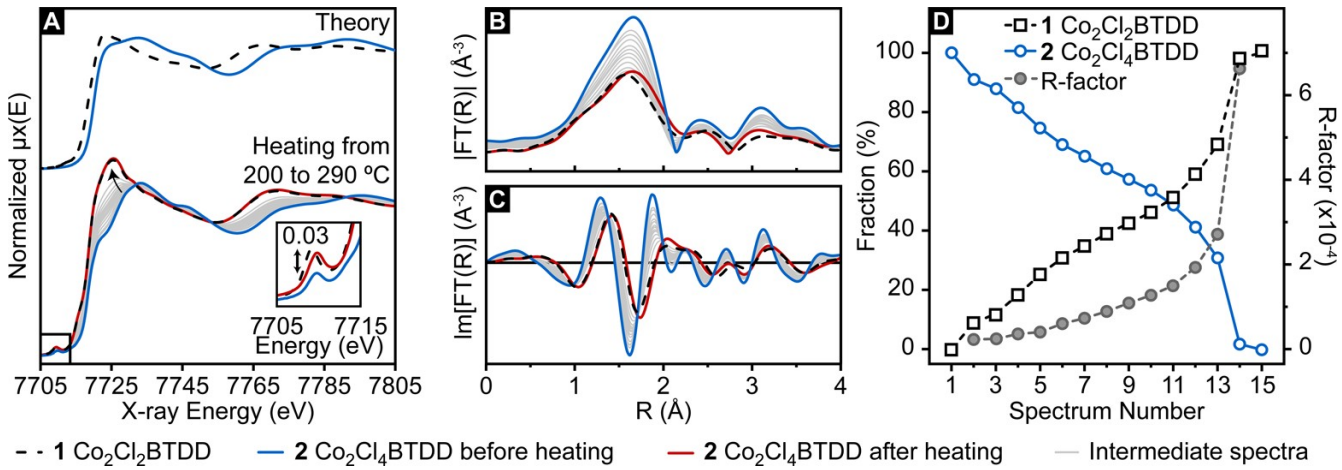

Figure 2. Co K-edge XAS characterization of 1 and 2: (A), top: Theoretical XANES spectra for **1** and **2** calculated from the NPD structures; bottom: Experimental XANES spectra at RT for **1**, **2**, **2** after heating, and intermediate states collected in the 200-290 °C range during the thermal treatment of **2**; the inset shows a magnification of the pre-edge peak at ca. 7709 eV. (B) magnitude and (C) imaginary parts of the phase-uncorrected Fourier-transformed k^2-weighted EXAFS spectra, FT(R). (D) Linear combination analysis of the whole series of *in situ* XANES spectra using the spectra of **1** and **2** at RT as references: relative fraction (open symbols) and fit quality factor (full symbols).

Thermal release of elemental halogens from oxidized MOFs

Thermogravimetric analysis (TGA) of dry samples of **2** and **3** under a stream of He revealed surprisingly sharp weight loss steps at approximately 275 °C and 195 °C, respectively, and no subsequent weight losses up to approximately 450 °C (Figure 3). Compound **1** itself did not exhibit any weight loss up to 400 °C. This data suggested that **2** and **3** may eliminate elemental halogens thermally. Coupling the thermogravimetric analyzer with an in-line mass spectrometer confirmed this hypothesis. The ion flux, which peaked at temperatures coinciding with those promoting weight loss observed by TGA, primarily consisted of X_2^+ ions and ionized halogen decomposition products (further details in Supplementary information). For **2** the primary species were $^{35}Cl^+$ and $^{37}Cl^+$, as well as the corresponding hydrogen chloride isotopologs (Figure S10). Importantly, we also detected the masses of the two major isotopologs of Cl_2: $^{70}Cl_2^+$ (57.4% natural abundance) and $^{72}Cl_2^+$ (36.3% abundance). For **3**, we observed all three isotopologs of molecular bromine: $^{158}Br_2^+$, $^{160}Br_2^+$, and $^{162}Br_2^+$ with their expected natural abundances (25.7%, 50.0%, 24.3%, respectively), as well as their decomposition products: ionized bromine atoms and hydrogen bromide ions (Figure S11).

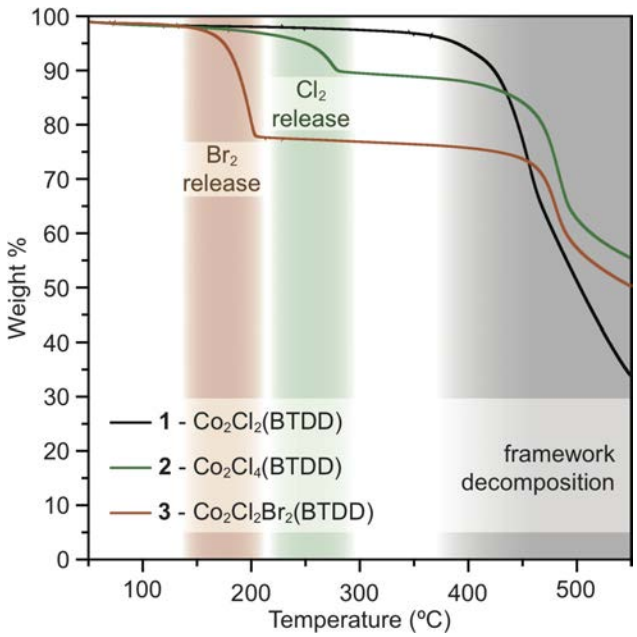

Figure 3. Thermogravimetric analyses. The TGA plot of **1** (black line) shows that framework decomposition occurs at *ca.* 400 °C. Abrupt weight loss, corresponding to halogen liberation from **2** (green line) and **3** (brown line) are emphasized in the green and brown regions, respectively.

Thermal elimination of X_2 from both **2** and **3** occurs without notable losses in crystallinity or porosity. PXRD analysis of **2** and **3** after halogen elimination by thermal treatment at 300 °C and 210 °C, respectively, revealed patterns that were identical to that of **1**, the all-Co(II) parent material (Figure S2). N_2 adsorption isotherms of thermally treated samples of **2** and **3** showed total uptakes of 550 cm^3/g and 660 cm^3/g, respectively (Figure S5). Both isotherms can be fitted to reveal very narrow pore size distributions peaking at 22.6 Å, again very close to the original value of 22.9 Å found in **1** (Figure S7). Together, the TGA and gas sorption data suggest that the majority of Co(III) sites in **2** and **3** are reduced to Co(II) upon thermal halogen elimination.

Further confirmation of the reversible uptake/release of halogens by **1** came from in situ XAS studies of Cl_2 elimination. Thus, following the Co K-edge energy while heating **2** from room temperature to 290 °C revealed essentially no change below 200 °C, and a progressive decrease between 200 °C and 290 °C. Additionally, the pre-edge absorption peak intensity at ca. 7709 eV increases upon heating, indicating a gradual conversion of the Co coordination geometry from octahedral to square pyramidal (Figure 2A). Linear combination analysis performed on the whole series of XANES spectra using the spectra of **1** and **2** at room temperature as references allowed us to quantify the transformation of **2** to **1** (Figures 2D, S17). The content of **2** decreased steadily from 91% at 207 °C to less than 2 % at 285 °C, where the position and shape of the XANES spectrum nearly coincided with that of **1** (Figure 2A). The higher residual signal and increased R-factor values observed at the highest temperature points suggest that the product obtained by thermal treatment of **2** is very similar to **1**, but exhibits a higher degree of static structural disorder relative to the latter. An equivalent trend is observed in the EXAFS spectra. The weakening of the EXAFS signal stemming from the Cl shell scattering (Figure 2B), as well as the progressive elongation of first shell bond distances, evident from the imaginary component (Figure 2C), are consistent with reducing the majority of MOF nodes from Co(III) to Co(II).

Although the *in situ* XANES data suggest that the conversion from **2** to **1** is nearly complete at the end of the thermal treatment (Figure 2D, left ordinate axis), the weight losses observed under the milder TGA conditions, 9.5 wt% and 21 wt% for **2** and **3**, respectively, correspond to elimination of only 70-80 % of the theoretical halogen content. Thermal treatment of bulk samples of **2** and **3** under vacuum gave products with elemental formulas of $Co_2Cl_{2.4}$BTDD and $Co_2Cl_2Br_{0.34}$BTDD, respectively, which also indicate loss of only approximately 80% of the releasable halogen content. Iodometric titration of Br_2 trapped from thermal treatment of **3** confirmed that the isolated yield of Br_2 under these conditions is close to 80% (Table S2). Importantly, the loss of Br_2 determined by iodometry never exceeded that observed by TGA, confirming that the species eliminated from **3** is indeed Br_2, and not lighter halogens, such as Cl_2 or BrCl, as might be expected if the original bridging chlorides were involved in the elimination. The apparent quantitative discrepancy between the TGA and XANES data stems from the average character of the XAS technique, which complicates the assignment of a minor fraction of unreacted Co(III) sites. Indeed, the spectrum of **2** collected after heating (spectrum 14, Figure 2D, right ordinate axis) has an R factor that is more than three times larger than those of the preceding sequential spectra collected during heating. The higher level of static disorder evidenced by EXAFS analysis of **2** after heating matches well with the possible presence of 10-20% of Co(III) sites that coordinate three Cl atoms in the first shell in a slightly distorted environment (see also Supporting Information Section 9.3).

Importantly, **1** can store and release halogens more than once: three consecutive cycles of exposing **1** to Br_2 vapors and thermal Br_2 release gave a reproducible recovery of 75-80% of the theoretical Br_2 yield with retention of structural integrity, crystallinity, and only minimal deterioration of porosity, as confirmed by SEM, PXRD analysis, and N_2 adsorption measurements after each cycle, respectively (Figures S3, S6). Altogether, these data suggest that a recovery yield of 80% is what should be expected in practice when using **1** for the reversible storage of halogens for the first cycle, with the yield becoming essentially quantitative on subsequent cycles.

Mechanistic considerations of X_2 release

The persistent 80% recoverable yield of halogens under cycling conditions is intriguing. It implies that there may be an inherent preference, thermodynamic or kinetic, for approximately 20% of the Co atoms in **2** and **3** to remain oxidized. To advance a hypothesis for this unexpected behavior, one may consider possible X_2 elimination mechanisms from **2** or **3**. These include formation and recombination of two X$^{\bullet}$ radicals, attack of X$^{\bullet}$ onto a terminal halide species, or the concerted formation of X_2 without the intermediacy of X$^{\bullet}$ (Figure 4A). Although the shortest distance between terminal halides is 6.5 Å and 6.8 Å for **2** and **3**, respectively, concerted X_2 elimination from these nearest intra-chain neighbors is physically impossible because the two X atoms point into neighboring pores, such that concerted formation of an X–X bond is obstructed by a structurally integral bridging Cl atom. There are several alternative pairs of terminal halide atoms that would allow elimination of X_2 (i.e. elimination would occur from within the same pore). However, the shortest X···X distance for these intra-pore elimination routes is
7.8 Å or 7.9 Å for **2** and **3**, respectively; too long for a concerted X_2 elimination mechanism (Figure 4B). Therefore, elimination of X_2 must occur through a radical mechanism, via homolytic cleavage of the terminal Co(III)–X bonds. What, then, prevents the complete conversion of all Co(III)–X species to Co(II) and quantitative formation of X_2?

To probe the thermodynamics of halogen release we employed density functional theory (DFT) calculations on a 1×1×2 expansion of the crystallographic unit cell, which yielded six unique Co centers per periodic chain. By sampling all possible elimination combinations, we find that generating pairs of immediately adjacent Co(II) centers occurs with no further energetic penalty relative to generating the first Co(II) center. In other words, elimination of an X atom from a Co(III)–X moiety immediately adjacent to an existent Co(II) center is thermodynamically favored relative to the formation of another isolated Co(II) center (Figure S23). The DFT model makes no inference on the fate of the departing halogen atoms, but rather considers the energetics of the residual dehalogenated Co chains. These computations therefore suggest that halogen release is pairwise through a mechanism shown schematically in Figure 4C. Further removal of halogens from our truncated model posed computational challenges (limitations are discussed in detail in the Supporting Information).

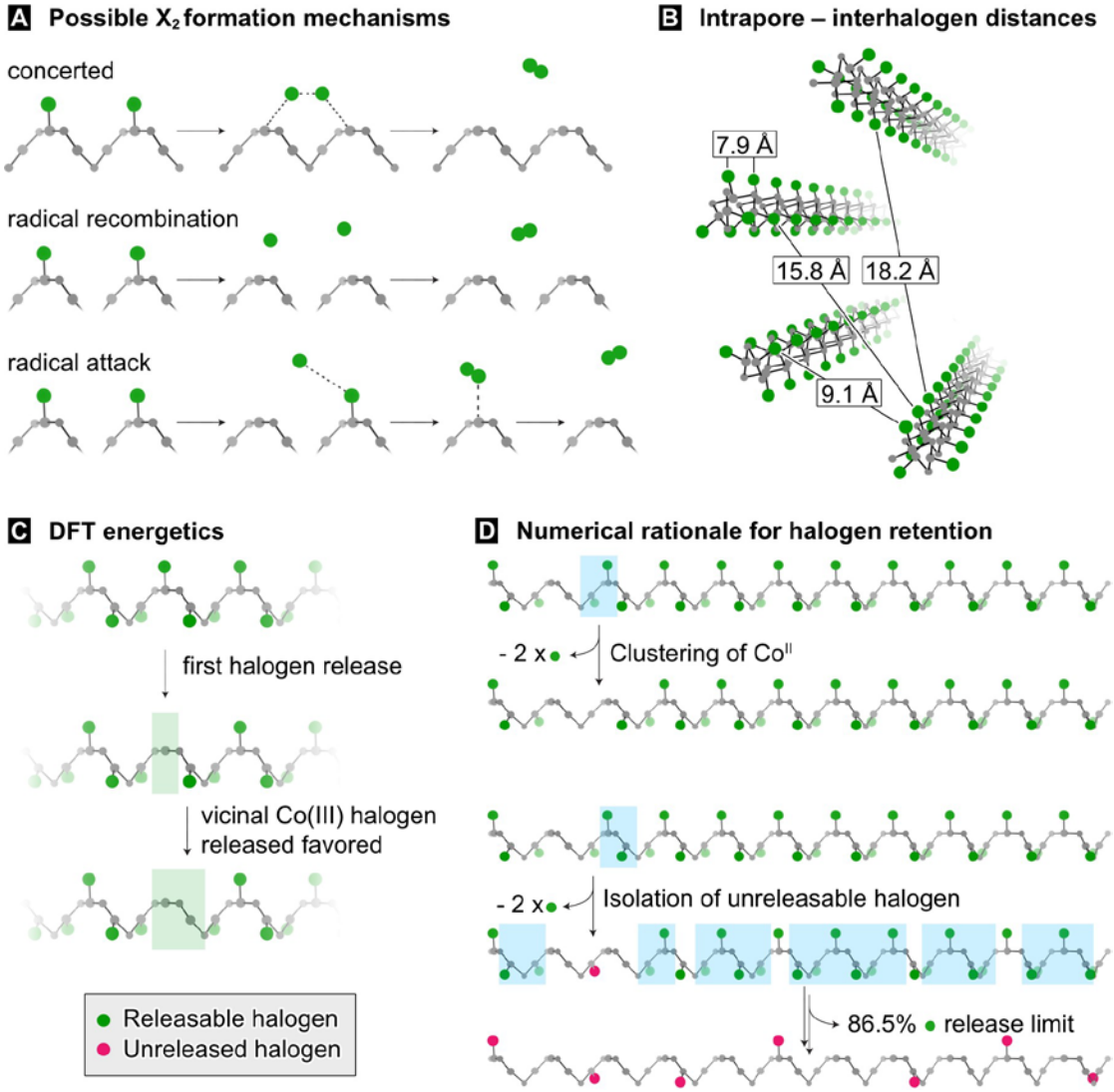

Figure 4. X_2 formation rationale. (A) Three possible mechanisms for the formation of elemental halogens. The concerted mechanism can be though to have formal radical character, whilst both the recombination and attack schemes feature transient X˙species. (B) The nearest intrapore halogen neighbors are separated by 7.9 Å. (C) DFT calculations predict vicinal removal of halogens is most favored. (D) A graphical representation of our probabilistic model for halogen removal depicting the route to the retention of 13.5% terminal halogens.

Combining the DFT result of nearest neighbor elimination and our experimental observation of formation of X_2, we can construct a probabilistic model in which random pairs of Co(II) centers are formed from an infinite chain of Co(III) centers, as shown in Figure 4C. With the only initial criterion being pairwise vicinal removal of halogens, this model predicts a residual Co(III)–X content of 13.5%, corresponding to halogen release of 86.5% of the theoretical maximum (complete mathematical derivation is presented in the Supporting Information). This is in remarkable good agreement with our experimental data, given the simplicity of our mathematical model and the size limitations of our computational model. Combining these models, we conclude that our experimental retention of approximately 20% of the terminal Co-bound halogens is exemplary of the high performance of **1** for reversible halogen capture and release.

CONCLUSIONS

Uptake of elemental halogens, Cl_2 and Br_2, by a robust Co(II) azolate MOF occurs without loss of crystallinity or porosity. Subsequent thermal treatment of the oxidized materials releases the elemental halogens, closing a cycle that amounts to reversible capture and release of these highly corrosive gases. This cycling behavior is unprecedented in MOFs, which are typically decomposed by or react irreversibly with the lighter halogens. The unusual reactivity here is enabled by the quantitative formation of Co(III) SBUs, also unique for MOFs, and the facile homolytic cleavage of Co(III)–X bonds[26] to form X_2 through a radical mechanism. These results provide a blueprint for the design of other porous materials geared towards the capture and storage of noxious, corrosive gases through reversible chemisorptive mechanisms.

Acknowledgements

Studies of metal−small molecule interactions in the Dincă lab are supported by a CAREER Award to M.D. from the National Science Foundation (DMR-1452612). M.D. acknowledges the Sloan Foundation, the Research Corporation for Science Advancement (Cottrell Award), and 3M for non-tenured faculty funds. We thank Dr. G. Agostini for assistance with the XAS data collection at ESRF BM23 and Dr. H. Müller for his support in the ESRF chemistry lab. C.L. and K.A.L. acknowledge the Mega-grant of the Russian Federation Government no. 14.Y26.31.0001. E.B. acknowledges Innovation Fund Denmark (Industrial postdoc no. 5190-00018B). We thank Mr. W. F. DiNatale at the Institute of Solder Nanotechnology (ISN) for assistance with SEM and Dr. C. Settens at the MIT Center for Materials Science and Engineering (CMSE) for assistance with capillary PXRD measurements. This work used the Extreme Science and Engineering Discovery Environment (XSEDE), which is supported by National Science Foundation grant number ACI-1548562.

REFERENCES

(1) Fauvarque, J. *Pure Appl. Chem.* 1996, *68*, 1713.

(2) McDonald, R. B.; Merriman, W. R. *Special Publication, Chem. Soc.* 1977, *31*, 168.

(3) Murray, L. J.; Dincă, M.; Yano, J.; Chavan, S.; Bordiga, S.; Brown, C. M.; Long, J. R. *J. Am. Chem. Soc.* 2010, *132*, 7856.

(4) Xiao, D. J.; Gonzalez, M. I.; Darago, L. E.; Vogiatzis, K. D.; Haldoupis, E.; Gagliardi, L.; Long, J. R. *J. Am. Chem. Soc.* 2016, *138*, 7161.

(5) Bloch, E. D.; Queen, W. L.; Chavan, S.; Wheatley, P. S.; Zadrozny, J. M.; Morris, R.; Brown, C. M.; Lamberti, C.; Bordiga, S.; Long, J. R. *J. Am. Chem. Soc.* 2015, *137*, 3466.

(6) Yang, S.; Sun, J.; Ramirez-Cuesta, A. J.; Callear, S. K.; David, W. I. F.; Anderson, D. P.; Newby, R.; Blake, A. J.; Parker, J. E.; Tang, C. C.; Schröder, M. *Nat. Chem.* 2012, *4*, 887.

(7) Britt, D.; Tranchemontagne, D.; Yaghi, O. M. *Proc. Natl. Acad. Sci. U. S. A.* 2008, *105*, 11623.

(8) Morris, W.; Doonan, C. J.; Yaghi, O. M. *Inorg. Chem.* 2011, *50*, 6853.

(9) Katz, M. J.; Howarth, A. J.; Moghadam, P. Z.; DeCoste, J. B.; Snurr, R. Q.; Hupp, J. T.; Farha, O. K. *Dalton Trans.* 2016, *45*, 4150.
(10) Rieth, A. J.; Tulchinsky, Y.; Dincă, M. *J. Am. Chem. Soc.* 2016, *138*, 9401.
(11) Marshall, R. J.; Griffin, S. L.; Wilson, C.; Forgan, R. S. *Chem. - Eur. J.* 2016, *22*, 4870.
(12) Brozek, C. K.; Dincă, M. *J. Am. Chem. Soc.* 2013, *135*, 12886.
(13) Xiao, D. J.; Bloch, E. D.; Mason, J. A.; Queen, W. L.; Hudson, M. R.; Planas, N.; Borycz, J.; Dzubak, A. L.; Verma, P.; Lee, K.; Bonino, F.; Crocellà, V.; Yano, J.; Bordiga, S.; Truhlar, D. G.; Gagliardi, L.; Brown, C. M.; Long, J. R. *Nat. Chem.* 2014, *6*, 590.
(14) Moen, A.; Nicholson, D. G.; Running, M.; Lamble, G. M.; Lee, J.; Emerich, H. *J. Chem. Soc., Faraday Trans.* 1997, *93*, 4071.
(15) Rossin, A.; Di Credico, B.; Giambastiani, G.; Peruzzini, M.; Pescitelli, G.; Reginato, G.; Borfecchia, E.; Gianolio, D.; Lamberti, C.; Bordiga, S. *J. Mater. Chem.* 2012, *22*, 10335.
(16) Cozzolino, A. F.; Brozek, C. K.; Palmer, R. D.; Yano, J.; Li, M.; Dincă, M. *J. Am. Chem. Soc.* 2014, *136*, 3334.
(17) Dietzel, P. D. C.; Morita, Y.; Blom, R.; Fjellvag, H. *Angew. Chem., Int. Ed.* 2005, *44*, 6354.
(18) Barrett, E. P.; Joyner, L. G.; Halenda, P. P. *J. Am. Chem. Soc.* 1951, *73*, 373.
(19) Kruk, M.; Jaroniec, M.; Sayari, A. *Langmuir* 1997, *13*, 6267.
(20) DeCoste, J. B.; Browe, M. A.; Wagner, G. W.; Rossin, J. A.; Peterson, G. W. *Chem. Commun.* 2015, *51*, 12474.
(21) Zhang, S.; Liu, X.; Liu, L.; Xia, Z.; Wang, W.; Yang, Qi.; Ke, H.; Wei, Q.; Xie, G.; Chen, S.; Gao, S. *Sci. China: Chem.* 2015, *58*, 1032.
(22) Wei, Y.; Chen, K.; Liao, P.; Zhu, B.; Lin, R.; Zhou, H.; Wang, B.; Xue, W.; Zhang, J.; Chen, X. *Chem. Sci.* 2013, *4*, 1539.
(23) Liao, P.-Q.; Chen, H.; Zhou, D.-D.; Liu, S.-Y.; He, C.-T.; Rui, Z.; Ji, H.; Zhang, J.-P.; Chen, X.-M. *Energy Environ. Sci.* 2015, *8*, 1011.
(24) Tonigold, M.; Lu, Y.; Bredenkötter, B.; Rieger, B.; Bahnmüller, S.; Hitzbleck, J.; Langstein, G.; Volkmer, D. *Angew. Chem., Int. Ed.* 2009, *48*, 7546.
(25) Lu, X.; Liao, P.; Wang, J.; Wu, J.; Chen, X.; He, C.; Zhang, J.; Li, G.; Chen, X. *J. Am. Chem. Soc.* 2016, *138*, 8336.
(26) Schrauzer, G. N.; Sibert, J. W.; Windgassen, R. J. *J. Am. Chem. Soc.* 1968, *90*, 6681.